Development of Simulation Technique for Crust Formation calculation using Rigid Body Dynamics Model in Moving Particle Semi-implicit

Yun Sik Cho(1) Ye Hwan Chun(1) Cheolwoong Kim(1) Sung Joong Kim(1, 2)
Department of Nuclear Engineering, Hanyang University (1)
Institute of Nano Science & Technology, Hanyang University (2)
yunscho@hanyang.ac.kr

1. Introduction

After Three Mile Island (TMI) and Fukushima accidents, safety analysis in severe accidents condition has become a major topic in nuclear research. During a postulated severe accident scenario involving failure of emergency core cooling, molten corium can be generated and released from the RPV, and behavior of the molten corium can influence the aspect of the severe accident scenario. Especially, as the crust layer may exist as obstacle of heat transfer and flow behavior at surface of the molten corium, calculation of crust formation behavior also major topic for prediction of severe accident scenario. Behavior of molten corium and solidification of crust layer have been studied through preceding studies. The studies mainly have been conducted through experimental studies and computational analysis including empirical correlation.

Many studies simulate behavior of molten corium by pouring molten corium into stainless-steel substrate. KATS [1], SPREAD [2], FARO [3] and VULCANO [4-6] was one of the representative spreading test facility using oxide simulant. The interpretation of heat removal and solidification by radiative heat transfer was sufficiently observable. While the experimental studies provide information for behavior of molten salt in a specified environment, the experimental studies have limit that they cannot evaluate behavior in various environments.

Many computational studies have also been conducted to predict the melt spread process. Firstly, MELT SPREAD [7], THEMA [8-9] and CORFLOW [10] were developed in Eulerian-based Lumped parameter codes, to simulate behavior of molten corium in severe accident scenario. The Eulerian-based numerical tools have advantages including high accuracy and calculation efficiency, but also have limit that it should rely on the above empirical formula and computational domain.

Lagrangian approaches can be more proper candidate for substitute to predict the phase change and thermal behavior in condition of various environment and changes in computational domain. Moving Particle Semi-implicit (MPS) which is one of the main Lagrangian-based simulation method, can provide high accuracy in fluid dynamics, heat transfer, and phase change of incompressible fluids for Corium analysis. The previous study [11] about corium analysis using MPS method has been sufficiently achieved, while interpretations still show a little high error rate caused by assumptions for changes in thermal properties in phase change of molten metal.

Thus, the objective of this study is development of heat transfer and phase change calculation technique in MPS which does not rely on empirical formulas. The calculated results were compared with data from some spread experiments and results of preceding numerical studies and to verify and validate the numerical model developed in this study.

2. Numerical Method

2.1. Governing Equation for MPS Method

MPS is one of the Lagrangian-based computational fluid dynamics (CFD) methods which means particle - tracking simulation methods developed to analyze incompressible fluid such as water or metals. The MPS calculates fluid dynamics using the interaction with neighboring particles existing within effective radius which is a certain distance radius from the calculating particles. For this purpose, Kernel function in equation (1) was used and it quantifies the degree of interaction over distance. without generating a computational grid, Lagrangian-based CFD employ numerical models using partial differential operators such as gradient, divergence and laplacian operators with Kernel function.

$$w(r) = \begin{cases} \frac{r}{r_e} - 1 & (0 < r \leq r_e) \\ 0 & (r_e \leq r) \end{cases} \quad (1)$$

The value r_e means effective radius, and r means distance between the computing particle and neighboring particles. The effective radius is determined by multiplying the average distance between particles with effective radius factors. If the factors get larger, as the particles get more interacting particles, computation has larger accuracy but more computational load. Thus, appropriate effective radius should be used.

While the MPS method basically calculates fluid dynamics using two kinds of equation, mass and momentum conservation for flow analysis, this study additionally treated Energy conservation to calculate heat transfer behavior and phase change of melt spread through Equations (2), (3) and (4).

$$\frac{\partial n}{\partial t} + \nabla \cdot (nu) = 0 \quad (2)$$

$$\frac{Du}{Dt} = -\frac{1}{\rho}\nabla P + v\nabla^2 u + F_{externel} \quad (3)$$

$$\frac{\partial H}{\partial t} = \frac{k}{\rho C_p}\nabla^2 H + q''' \quad (4)$$

2.1.1. Flow analysis model.

As mentioned earlier, the MPS method uses kernel function to represent partial differential operators to compute interactions with neighboring particles. Equations (5), (6) and (7) represent the gradient, divergence and Laplacian operators using Kernel function used in the MPS method, respectively.

$$\langle \nabla\phi \rangle_i = \frac{d}{n^0}\sum_{j\neq i}\left[\frac{\phi_j - \phi_i}{|r_j - r_i|^2}(r_j - r_i)w(|r_j - r_i|)\right] \quad (5)$$

$$\langle \nabla\cdot\phi \rangle_i = \frac{d}{n^0}\sum_{j\neq i}\frac{(\phi_j - \phi_i)\cdot(r_j - r_i)}{|r_j - r_i|^2}w(|r_j - r_i|) \quad (6)$$

$$\langle \nabla^2\phi \rangle_i = \frac{2d}{n^0\lambda}\sum_{j\neq i}(\phi_j - \phi_i)w(|r_j - r_i|) \quad (7)$$

The value, ϕ stands for the computational variable. n^0, d mean particle density and dimension, respectively. The subscript i and j represent the computing particle and neighbor particle. λ means kernel radius, the main factor used in the Laplacian calculation, which is the average value of multiplying radius with kernel function as shown in equation (8).

$$\lambda = \frac{\int_V w(r)r^2 dv}{\int_V w(r)\, dv} \quad (8)$$

As mentioned earlier, the MPS method calculates flow analysis by developing numerical models of equation (2) and (3) using partial differential operators of equation (5) and (6). In this process, equation (2) and (3) are divided into Explicit Step and Implicit Step, and a temporary step is built for this purpose as an intermediate term.

As shown in equation (9), the explicit step computes the velocity vector of the temporary step using terms of convection and external force in the right-hand side of equation (3).

$$u^* = u^t + \Delta t\left[\frac{2d\nu_{ij}}{n^0\lambda}\sum_{j\neq i}(u_j - u_i)w(|r_j - r_i|) + F_{externel}\right] \quad (9)$$

$$\nu_{ij} = \frac{2\nu_i\nu_j}{\nu_i + \nu_j} \quad (10)$$

Thus, the coefficient, ν_ij in equation (10) was used as effective kinematic viscosity which is harmonic average between kinematic viscosity of each particle.

On the other hand, in the implicit step for flow calculation, equation (11) calculates laplacian pressure using the pressure gradient term in equation (3), Navier Stokes equation.

$$\nabla^2 P^{n+1} = \frac{\rho}{\Delta t}\langle \nabla\cdot u^* \rangle_i \quad (11)$$

The following equation (12) is also derived by combining equation (11) and continuity equation, in equation (2).

$$\nabla^2 P^{n+1} = \frac{\rho}{(\Delta t)^2}\frac{n^* - n^0}{n^0} \quad (12)$$

While the equation (12) alone is also enough to calculate flow calculation, the pressure field was calculated using multi-source term model [12] in equation (13) by adding equation (11) and equation (12) combined with the divergence operator for computational stability.

$$\langle \nabla^2 P \rangle_i = \alpha_1\frac{\rho}{\Delta t}\langle \nabla\cdot u^* \rangle_i + \alpha_2\frac{\rho}{(\Delta t)^2}\frac{n^* - n^0}{n^0} \quad (13)$$

$$\langle \nabla^2 P \rangle_i = \frac{2d}{n^0\lambda}\sum_{j\neq i}(P_j - P_i)w(|r_j - r_i|) \quad (14)$$

The factors, α_1 and α_2 in the above equation represent weights for each equation (11) and (12). As sum of the α_1 and α_2 value should be one, 1.0 and 0.05 was used for each value. In this study, we successfully conduct implicit computation for equation (13) and (14) by using linear algebra, Conjugate Gradient method [13] for matrix calculation.

2.1.2. Heat transfer model.

Numerical models for heat transfer calculation in MPS are interpreted by heat transfer on interfaces between two particles. The model was derived by modifying the energy conservation equation of equation (4) using the laplacian operator of equation (7).

$$H^* = H^t + \Delta t\left[\frac{2k_{ij}d}{\rho C_p n^0\lambda}\sum_{j\neq i}(H_j - H_i)w(|r_j - r_i|) + q'''\right] \quad (15)$$

The mean value of thermal resistance of each two fluids or solid materials was used as thermal resistance on the interfacial boundary. Thus, the coefficient, k_{ij} was used as effective conductivity which is harmonic average between thermal conductivity of each particle because it is inverse of thermal resistance.

$$k_{ij} = \frac{2k_i k_j}{k_i + k_j} \quad (16)$$

In this study, the phase transition was determined by the enthalpy value which is calculated with equation (15).

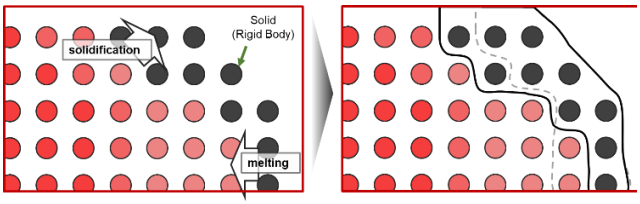

Fig. 1. Rigid body grouping after phase change

In this study, when the heat transfer calculation result shows solidification or melting, the Rigid body group is designated as shown in the figure above, and the Rigid body analysis is performed according to 2.1.3.

2.1.3. Rigid body dynamics model.

Rigid Body Dynamics model was developed to calculation behavior of solid mass operating within the MPS code such as crust layer.

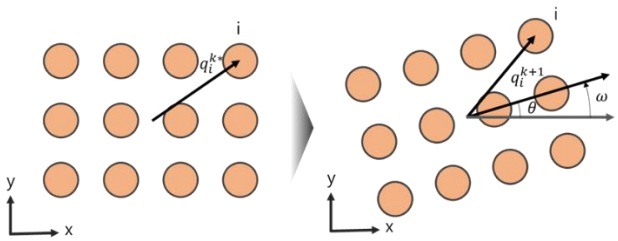

Fig. 2. Relative coordinates in rigid body mass

As shown in Fig 1 and equation (17) to (19), particles within the rigid body mass move as a mass and move with same speed,u_g and a constant relative coordinate, q_i^{k*}.

$$r_g = \frac{1}{N}\sum_i^N r_i \quad (17)$$

$$q_i^{k*} = r_i - r_g \quad (18)$$

$$u_g = \frac{1}{N}\sum_i^N u_i^{k*} \quad (19)$$

2.1.4. Boundary condition

Before calculation with the MPS method, Free surface, which is particles near the void, should be detected using condition with particle number density (n_i). If the particle number density of the target particle is lower than the threshold which is average particle number density multiplied with free surface coefficient (β) and β was set up as 0.95 in this study.

$$n_i < \beta n_0 \quad (20)$$

Heat loss mainly occurs at the free surface through radiation heat transfer. Equation (21) shows radiation model based on Stefan-Boltzmann's law where ε is radiation emissivity, σ is Stefan-Boltzmann constant, A is surface area which determined only at the free surface particles.

$$Q = \varepsilon\sigma A T_i^4 \quad (21)$$

$$A = 6\left(1 - \frac{n_i}{n_0}\right) l_0^2 \quad (22)$$

3. Result

The FALO L-26S test, which was conducted in Karlsruhe, Germany in 1997, was analyzed using the 2D MPS code developed in this study. In this experiment, melted UO2/ZrO2 (the weight percentage of 80/20) about 160 kg was dropped by gravity through a drain tube of dry stainless-steel plates. The test was conducted at the FARO facility. The stainless-steel drain tube diameter is 150 mm, and the length of the lower spreading plate is 3050 mm, which is connected to the FARO furnace through the discharge tube, cross valve unit and discharge container. The 40 mm-high weir divided the drain tube from the spreading plate. About 190 kg of molten solution was generated and released to the test section via the discharge tube by gravity. The upper test condition was described as an input statement for MPS calculation and it was illustrated in Fig 3.

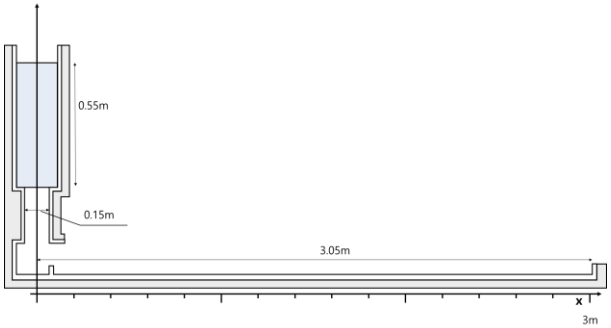

Fig. 3. Simple description of FARO Test

The UO2/ZrO2 mixture used in the FARO experiment was molten using electrodes prior to the experiment. Temperature measurements were conducted in the drain tube to measure the initial temperature. Initial conditions of the test sections were set up with initial temperature about 2950 K and atmospheric pressure.

The MPS calculation was successfully conducted with about 30 hours computation time to perform the calculation of 10 sec for flow analysis of 3,741 particles. The adaptive time step was set to about 0.0001 sec to

sufficiently reduce the error for each step, resulting in 10^{-6} of conjugate gradient calculation error.

The calculation results were derived using previously developed algorithm and input conditions, and the spreading length was calculated for proper comparative analysis. The spreading length which means maximum x-direction position of the core melt is compared with the result of preceding study and FARO-L26S experiment in Fig 4.

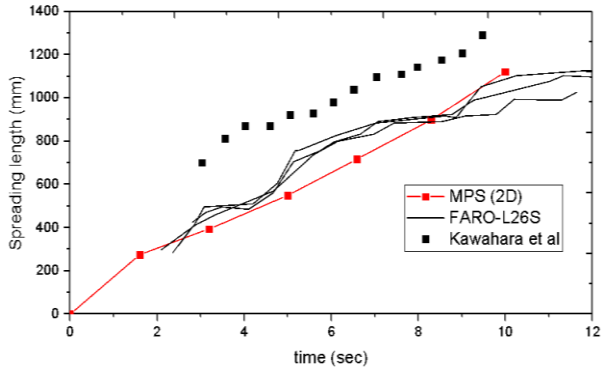

Fig. 4. Comparison with experimental results

Black solid lines in the figure indicate experimental result, black pointed data indicate result of preceding MPS study, and red solid line with point data indicate the calculation result in this study.

The computational results show linear tendency of spread behavior up to 10 seconds, with 1120 mm of spreading length at 10 seconds. The result showed lower error than previous study, which means that the flow analysis in this study has high stability and accuracy with given input conditions performed in this work. On the other hand, while the experimental result and preceding study shows a clear multistage curve with convex and concave curvature, the curve was not shown in this study. It is because, while the multistage curve can be caused by repeated solidification and melting process, sufficient solidification was not shown in this study. Fig 5 shows the morphology of spreading and solidification behavior with 2D MPS calculation.

As mentioned above and shown in the Fig 5, the crust formation from solidification was not generated enough, and it seems that heat transfer from the bottom of the spreading plate and radiation transfer at the upper boundary of the melt have not occurred sufficiently. As a result, modification on the heat removal model in wall heat transfer and radiation heat transfer will be needed through future works.

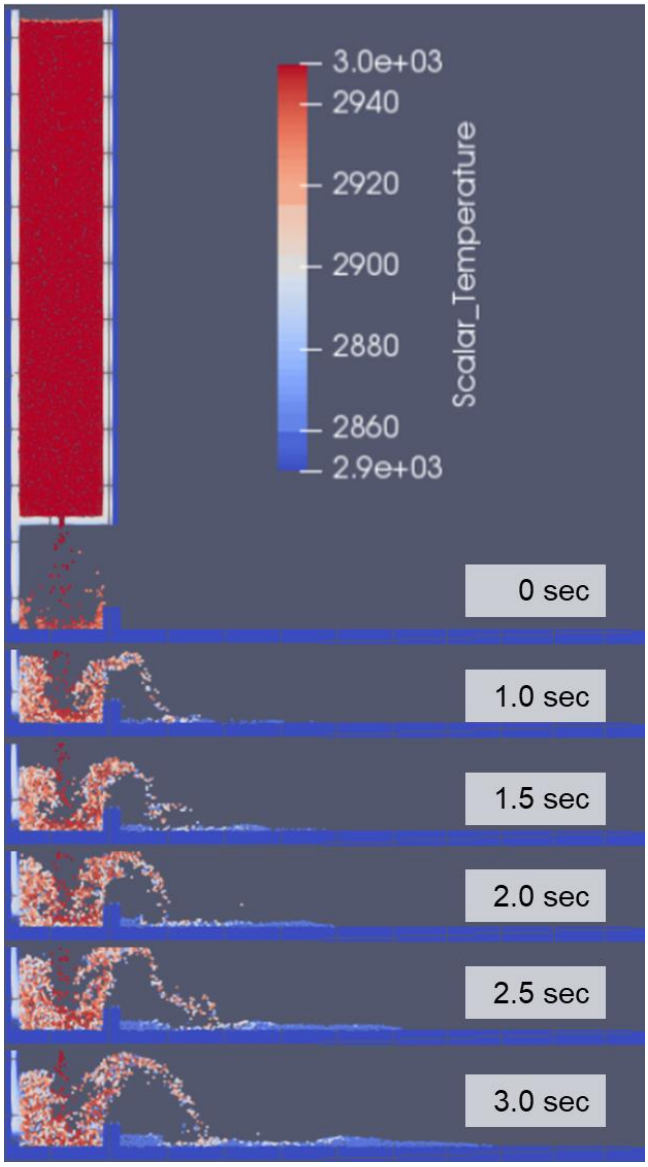

Fig. 5. Morphology of spreading behavior of corium mixture with 2D-MPS calculation.

4. Conclusions

Spreading behavior was measured using Moving particle semi-implicit method with modified algorithm which was developed by adding heat transfer computations to compute solidification, ablation, and re-melting phenomenon. The development of the algorithm was validated using data from of FARO L26S experiments. The computation was successfully performed with enough low error rates and high convergence. The computational results showed that the flow analysis model showed high stability and accuracy, while the heat transfer model can not generate enough crust, and it seems that additional modification was required in further study.

5. Acknowledgments

This research was supported by the National Research Foundation of Korea (NRF), funded by the Ministry of Science, ICT, and Future Planning, Republic of Korea (No. NRF- 2021M2D2A2076382)

6. Reference

[1] G. Engel, “KATS experiments to simulate corium spreading in the EPR core catcher concept.” No. FZKA--6475. (2000).
[2] J. J. Sienicki and M. T. Farmer, “Spreading of molten corium in Mk I geometry following vessel meltthrough”. No. CONF-881011-34. Argonne National Lab, IL, USA (1988)
[3] W. Tromm, J. J. Foit, and D. Magallon. “Dry and wet spreading experiments with prototypic material at the FARO facility and theoretical analysis.” No. FZKA--6475. (2000).
[4] J. Christophe, "Ex-vessel corium spreading: results from the VULCANO spreading tests." Nuclear Engineering and Design. 223(1) pp. 75-102 (2003)
[5] J. Christophe, "The VULCANO VE-U7 Corium spreading benchmark." Progress in Nuclear Energy. 48(3) pp. 215-234 (2006)
[6] J. Christophe, “Two-dimensional interaction of oxidic corium with concretes: The VULCANO VB test series.” Annals of Nuclear Energy. 36(10), pp. 1597-1613 (2009)
[7] M. T. Farmer, “Melt spreading code assessment, modifications, and application to the EPR core catcher design. " Atomic Energy Society of Japan, No. ANL-09/10, Argonne, IL, United States, (2009)
[8] B. Spindler, and J. M. Veteau. "The simulation of melt spreading with THEMA code: part 1: model, assessment strategy and assessment against analytical and numerical solutions." Nuclear engineering and design. 236(4), pp. 415-424 (2006)
[9] B. Spindler, and J. M. Veteau. "The simulation of melt spreading with THEMA code: Part 2: Assessment against spreading experiments." Nuclear engineering and design. 236(4) pp. 425-441 (2006)
[10] R. Wittmaack, "Corflow: a code for the numerical simulation of free-surface flow." Nuclear technology. 119(2), pp. 158-180 (1997)
[11] T. Kawahara, "Ex-vessel molten core solidification behavior by moving particle semi-implicit method." Journal of nuclear science and technology 49(12), pp. 1156-1164 (2012)
[12] H. Ikeda, "Numerical analysis of fragmentation processes of liquid metal in vapor explosions using moving particle semi-implicit method." Nippon Kikai Gakkai Ronbunshu. 64(624), pp 2431-2437. (1998)
[13] J. R. Shewchuk, "An introduction to the conjugate gradient method without the agonizing pain." (1994)
[14] S. J. Stedman, J. R. G. Evans, and J. Woodthorpe. "Rheology of composite ceramic injection moulding suspensions." Journal of materials science. 25(3), pp. 1833-1841. (1990).